2014 International Conference on Manipulation, Manufacturing and Measurement on the Nanoscale (3M-NANO)
27-31 October 2014, Taipei

Near Field Microwave Microscopy for Nanoscale Characterization, Imaging and Patterning of Graphene

Investigation on CVD grown graphene

Tamara Monti, Andrea Di Donato, Davide Mencarelli, Giuseppe Venanzoni, Antonio Morini, Marco Farina
Dipartimento di Ingegneria dell'Informazione (DII)
Università Politecnica delle Marche
Ancona, Italy
m.farina@univpm.it

Ivan V. Vlassiouk, Alexander Tselev
Oak Ridge National Laboratory
Oak Ridge, Tennessee

***Abstract*—This paper reports images of reproducible nanopatterns on hexagonal graphene flakes, produced by modulating the input power of a Near-Field Scanning Microwave Microscope, used at the same time for the characterization of the samples. We have studied the impact of different time exposures to the microwave field, and of different power levels. A possible explanation of the patterning mechanism is given by the heating-induced oxidation of the exposed graphene flakes. In order to confirm this assumption, we have developed a simplified model for the analysis of the heat distribution, and for the estimation of the temperature under the microscope probe. This effect could be the basis for an alternative nanolithographic technique.**

Keywords—component; Graphene; Nanolithography; Nanopatterning; Scanning Probe Microscopy

I. INTRODUCTION

During the last years, a wide variety of nanolithographic techniques have been applied to mono- and few-layers graphene, in order to manipulate and shape it. Graphene nanolithography is important not only for the realization of devices [1], but also for verifying and exploring properties and capabilities of this new material [2-6].

The most commonly used technique, sometimes considered as a standard for graphene applications, is the electron-beam (e-beam) lithography [7]. This can be combined with High-Resolution Transmission Electron Microscopy (HRTEM) for simultaneous monitoring of the effect of electron sputtering. In order to lower the required electrons power, e-beam lithography has been combined with sharp tips, used as contact electrodes [8]. An "ice-assisted" e-beam lithography application has also been proposed [9], where a thin ice layer covers graphene and low-energy e-beam is used.

The oxygen plasma etching [10], which can be coupled with optical lithography [11], is a common tool to create controlled patterns on graphene as well. Different kinds of ion etching, such as e.g., helium ion beam [12], or reactive ion etching [13], have also been successfully employed. Further, some works proposed block copolymer lithography [14] as well as the usage of metallic etchmasks [15].

Different kinds of photolithography have also been applied to graphene. In addition to [11], an example can be found in [16], where a confocal microscope was used. In [17] and [18] different lasers were exploited to directly write a pattern on a graphene flake.

Chemically-aided techniques have been widely explored, by means of the substrate morphology [19], [20], or with the help of additional nanoparticles [21], [22], [23]. As a matter of fact, several kinds of nanostructures have been used: graphene patterning has been achieved by exploiting nanospheres [24], [25], nanowires [26], or a more generic nanoimprint lithography [27]. All these techniques are based on chemical modification of the graphene surface. The majority of them exploits heating to induce such modification. By the same token, some authors proposed high-temperature oxidation [28], thermo-chemical lithography [29], etc. Photochemical processes are also employed through UV radiation [30], and under extreme conditions [31].

A completely different class of techniques, relevant for the graphene nanopatterning, is usually labeled as Scanning Probe Lithography (SPL) [32]. Interestingly, such techniques are based on microscopy techniques, having imaging resolutions in the order of nanometers or better. For the sake of completeness we should stress that, although the HRTEM and Scanning Transmission Electron Microscope (STEM) [33] could be in principle classified in the SPL group, they are conventionally associated to e-beam technique, as a particular class of high-energy lithography. Among the SPL methods, the most common are the Scanning Tunneling Lithography (STL) [34], the Atomic Force Lithography (AFL) [35], [36], [37], and the dip-pen lithography [38]. They can be collected together in a "tip-based" class of nanofabrication methods [39], where the nature of interaction between tip and graphene sample represents the peculiarity of a specific technique [40]. Tip and

978-1-4799-7923-3/14/$31.00 ©2014 IEEE

samples can interact in very peculiar ways, as reported for some classes of conjugate polymers [41].

In this work we report imaging, characterization and some etching effects produced by the interaction between a microwave near-field probe and the sample of interest, partially reported in [42]. As a highly interesting application of the above effects, the patterning of graphene grown by Chemical Vapor Deposition (CVD) is demonstrated.

While the exact physical mechanisms underlying the etching are still not completely clear, a detailed analysis of the possible thermal and electromagnetic phenomena involved in the process is presented and alternative possible explanations are addressed.

II. Microwave Microscopy

Our Scanning Microwave Microscope (SMM) was extensively described elsewhere [43], and already used by the Authors to measure some physical properties of the samples [44], according to past works [45]. Here we only report a brief summary of the working principles of the microscope as well as the nature of the electromagnetic interaction.

The Near-Field (NF) SMM is a particular SPM technique based on the interaction between a scanning metallic probe and the sample, illuminated by an electromagnetic field at microwave frequency. Since the interacting field is in the reactive region (near-field), in order to overcome standard imaging limits related to the wavelength, it is necessary to keep the distance between tip and sample within the nanometric range. Typically this is ensured by a feedback system based on Atomic Force Microscope (AFM) [46], microwave signal [45], or Scanning Tunneling Microscope (STM), as in the present case. In our microscope, in fact, the same metallic sharp tip is shared with a STM system to record simultaneously both the tunneling current between tip and sample and the microwave complex reflection coefficient (Fig. 1). It is then possible to pick-up information on the electronic structure and topography from STM as well as on the electromagnetic features (e.g. dielectric permittivity, conductivity) of the sample. The two measurements are carried on two separated channels, without mutual interference.

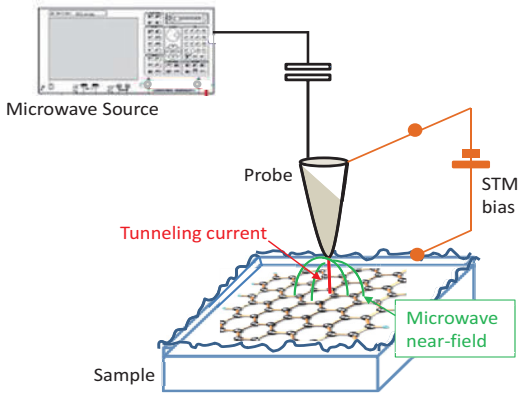

Figure 1. Scheme of the main elements of the NFSMM in use. The microwave field is guided from the source to the probe. A network analyzer records the reflected signal from the sample. Between tip and sample, an STM bias voltage is applied. The instrument performs STM imaging as well.

The microwave signal is guided from the source to the scanning tip by a coaxial cable. The tip acts as a radiating antenna, but, since the sample is located within the reactive near-field region, the electromagnetic interaction can be approximately considered in a quasi-static regime. Due to the features of our microscope, the power of the microwave source can be arbitrary regulated within the limit of +5dBm in the present implementation, and still ensures a good coupling with the metallic probe. In this way, the electromagnetic field interacting with the sample is maximized and local lithographic effects of selected samples have been observed, as discussed in the following. For SMM imaging the typically used source power is -15dBm, while we have observed patterning effects nearby the maximum power limit of our instrument, namely +5dBm (3.16 mW). This happens within the range of frequencies where the microscope has the best imaging performances. Most of the results discussed here are obtained nearby 16 GHz, while our microscope usually operated efficiently up to 25 GHz.

Remarkably, the minimum size of the patterned shapes is of the order of the resolution of the microscope itself. As a matter of fact, the maximum interaction is limited to a small volume of sample right under the apex of the tip, owing to the small curvature radius of the STM probe, creating a nearly singular electric field. Past works referred to this volume as a “sampling volume” [47] and it is essentially influenced by the size of the apex of the metallic tip. In principle it should be possible to obtain very narrow scratches with an optimized procedure, since SMM allows atomic resolution [48].

III. Graphene Samples

The samples under analysis consist of single layer graphene flakes over polycrystalline copper substrate. They are prepared by a CVD procedure, extensively described elsewhere [49]. Due to the particular thermal and pressure conditions in use, the shape of the graphene flakes is hexagonal, making samples identification through SPM quite easy. Some flakes are composed of multiple layers, but the great majority consists of single layer sheets. In order to make them visible to traditional optical microscopes, the samples have been slightly oxidized in air, so that the copper free from the graphene is covered by a thin layer of copper oxide. As recently reported in literature, it is most likely that, due to the conservation in an environment with non-controlled pressure and temperature conditions, a thin layer of copper oxide is able to grow also under the graphene flakes [50], in spite of its passivation. Furthermore, parts of the samples appear as highly corrugated, probably because of the difference between the temperature strain coefficients between copper and graphene [51].

IV. Microwave Patterning

We have observed a first evidence of microwave induced patterns at extremely low power (-15 dBm); in Fig. 2 a sequence of scans, evidencing this phenomenon, is reported. It shows an isolated graphene flake before and after two following SMM scans.

The scanned area measures 20 µm each side, containing a hexagonal flake of CVD graphene. The sample appeared as a

fairly smooth flake over a highly corrugated copper substrate. The first microscope scan took approximately 1 hour. Since the chosen resolution was 256x256 pixels, each spatial point of the square has been exposed to microwave power for about 55 ms. After that, the sample appeared modified, clearly showing two damages propagating from the edges of the hexagon. Then the sample area was exposed again to the same process, resulting in a deeper modification of the flake, at the destruction limit. The copper substrate underneath became visible.

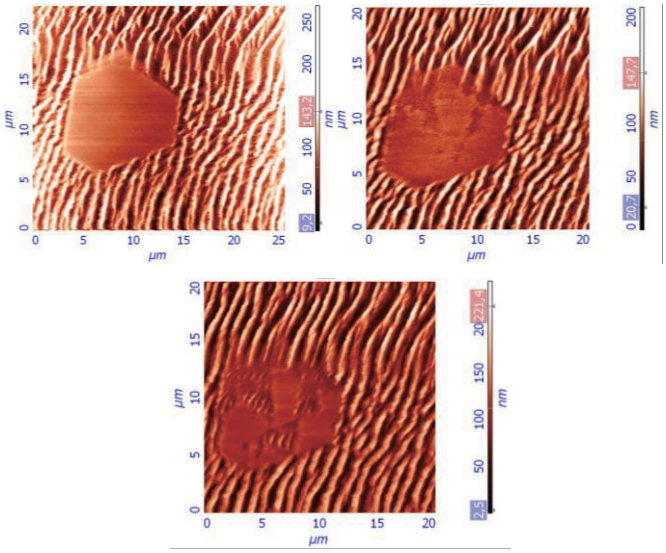

Figure 2. From the top left corner (clockwise): STM image of a graphene flake before SMM scans; STM image after the first scan; STM image after the second scan.

One should consider that, in addition to the microwave field, tunneling current flows between the metallic probe and the sample. Although the STM has been employed elsewhere for graphene patterning through selective oxidation [34], the voltage used for that purpose is significantly higher (several Volts) than our biasing values ($\approx$ 0.3 V). Therefore, while it is possible that STM and SMM impact may be concurring, from preliminary analysis (performing STM scans alone and scans with different microwave power) we ascertained that the main contribution comes from the microwave field. The fact that the phenomenon was observed with so modest microwave power was attributed to two special conditions: a) the flake lies over a very corrugated part of the copper substrate and b) the effect started from the flake edges, where unbound carbons can oxidize more easily.

In order to separate the contributions of tunneling current and microwave field on the surface modification, a set of experiments was performed: changing the microwave exposure time and power, as well as the STM bias voltage and the scanning duration. We report in Fig.3 the effect of successive STM and SMM scans, with different source power. Analogous procedure has been adopted to understand the effect of changing STM set-point and bias voltage. This confirmed that the most relevant effect on samples is due to the increasing microwave power that is able to completely remove the graphene hexagons from the substrate. In the meanwhile the scans also modify the copper substrate, as reported in Fig.3.

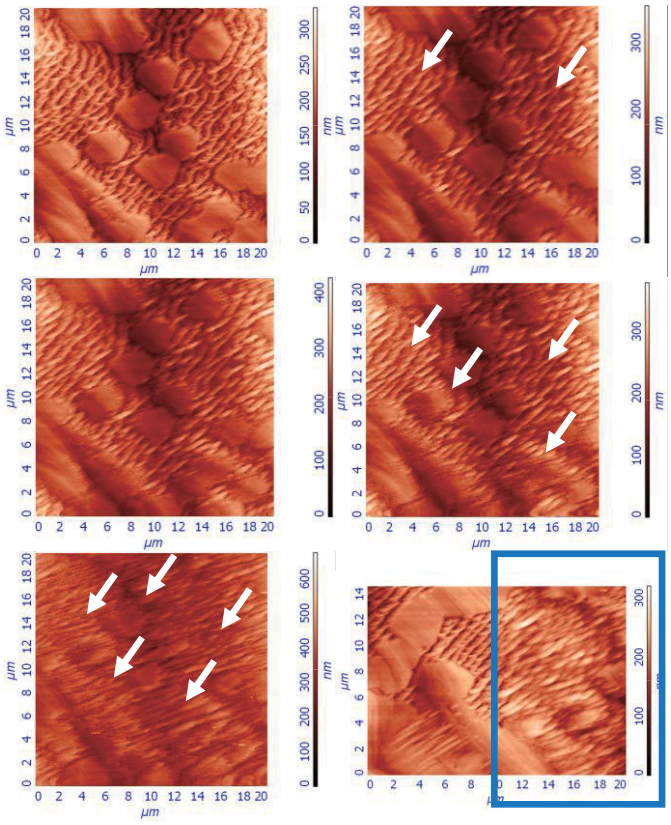

Figure 3. First row: images related to the same area of the sample after STM scans only.The white arrows highlight few changes in the Cu substrate. Second row (left) after a consecutive 1h10' tunneling + (-15dBm) microwave exposure; (right) after a consecutive 1h10' tunneling+ (0dBm) microwave exposure; third row (left) after a consecutive 1h10' tunneling+ (5dBm) microwave exposure. The white arrows highlight substantial changes both in the Cu substrate and in the graphene hexagons.In the bottom right image the highlighted area is the exposed one, seriously damaged with respect to the region nearby.

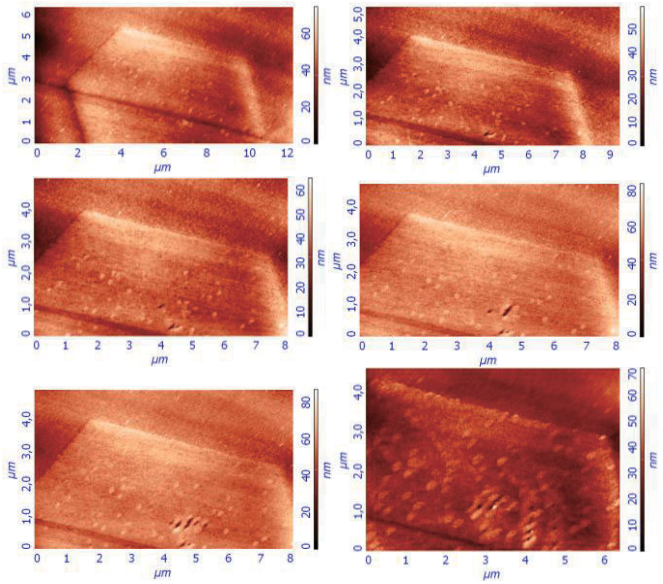

Figure 4. Sequence of STM images of a graphene hexagon: the patterning (a series of holes subsequently appearing in each image) has been created by (+5dBm) microwave exposure for 5' for each hole.

Then we exploited the microwave exposure to selectively etch the graphene flake, as reported in Fig. 4 and 5. In some experiments the probe has been kept at a fixed position: with a longer exposure time a line pattern has been obtained (Fig. 5), due to the residual drift of the piezoelectric nanopositioner.

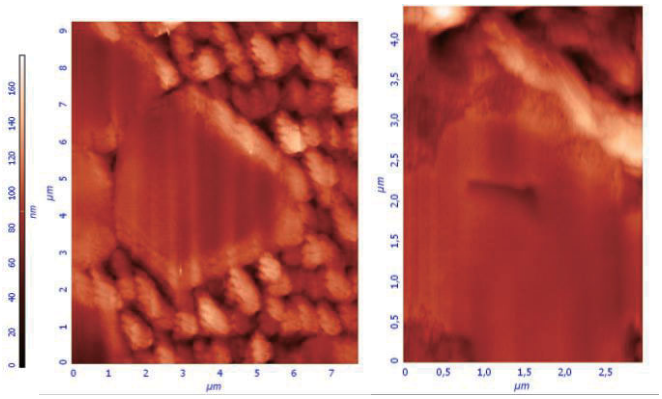

Figure 5. STM images of a flake before and after a (0dBm) microwave exposure for 1h. The drift of the instrument produced a line pattern.

Before discussing possible explanation of the observed graphene modification, we note that it is known that the local heating of the graphene makes patterning possible owing to the chemical interaction of carbon atoms with water molecules in air (oxidation). At the same time, graphene can directly interact with environmental oxygen molecules. Therefore, as a possible explanation, it is likely that the graphene etching is caused by microwave heating and following chemical modification of the surface. The electromagnetic field increases the local temperature of the sample area right under the tip, where it is extremely focused. Since the experiments are performed in air, the temperature increase triggers the chemical modification of the surface.

There are several observations, supporting this interpretation. Namely, depending on power level and exposure time, the effects can be modulated: in Fig. 3, as the whole area has been exposed, the graphene has been gradually removed, starting from the edges, where carbon atoms are weakly coupled. In the meanwhile, the copper substrate has been modified, probably increasing the surface oxide thickness. In this case, the exposure time was few tens of ms for each spatial point, during a raster scan. Each point is close to the other in both space and time, so the heating effects persist due to the proximity of the radiating source. In turn, in Fig. 4 and 5 the tip is kept in a fixed position (but the sample slightly moves underneath, because of the residual drift of the piezoelectric positioner) for a limited exposure time, respectively 5' each holes and 1 hour for the entire line. The exposure time seems extremely important, since it is not possible to obtain neither a hole nor a scratch of the graphene flake, without waiting for a prolonged while. It points to a heating-induced oxidation effect. For the experiments shown in Fig. 4, exposures shorter than 5 minutes did not cause any modification of the surface. The microwave power has a fundamental role in the etching process as well. Before obtaining the line pattern of Fig. 5, other parts of the same flakes have been exposed with lower power densities, without modifications. We conclude, that the mechanism needs a minimum kick-off power to start, and then a certain exposure time is necessary to clearly see the cumulating effect of the chemical changes.

After patterning the graphene flake, we moved the tip on the area of the oxidized copper substrate highlighted in Fig. 6. The microwave exposure time and power being the same as for the graphene case, interestingly, the etching was successful also on copper oxide.

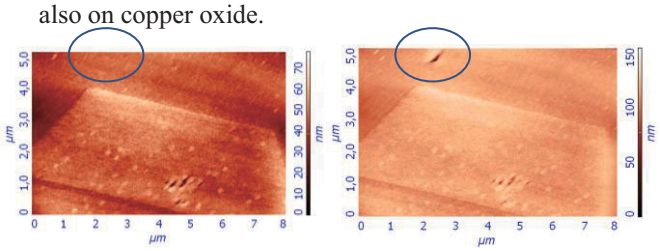

Figure 6. STM images before and after (+5dBm) microwave exposure for 5' on the oxide surface (highlighted by the blue circle).

V. SIMPLIFIED THERMAL MODEL

In order to evaluate the level of magnitude of the local temperature increase of the sample, a simplified situation is analyzed [52]. All the power not reflected back to the vector network analyzer (microwave source) is considered to be absorbed by the sample. Due to the high focusing capability of the tip apex, we assume that the microwave power is distributed over a sphere, having the same curvature radius of the probe itself [42], inside of the heated material (red in Fig. 7). Then, another external sphere (blue in Fig. 7) represents the volume of interaction with the surrounding material. Beyond this sphere the temperature is in equilibrium with the environment (in our case 300K).

Since the heat transfer by the air is negligible with respect to the conduction through solid materials (i.e. copper oxides and copper), the difference of temperature between the inner and outer sphere could be approximated to

$$\Delta T = Q[1/(4\pi k_{ox})\,(1/R_1 - 1/R_2) + 1/(4\pi k_{Cu})\,(1/R_2 - 1/R_3)]$$

where Q is the transferred power, k_{ox} and k_{Cu} are respectively the thermal conductivity of the copper oxide and copper, and R_1, R_2 and R_3 are defined as in Fig. 7. The effect can be understood by considering a simple resistive equivalent circuit. If the transferred power is focused in a sphere having a radius smaller than the thickness of oxide layer, the heat is dissipated by the oxide firstly, and by copper then. In this particular situation, because of thermal properties of the two materials, and because of the very small size of the spheres of interaction, the temperature on the surface could reach in principle a very high value. It can be compared to a high "voltage" drop in the equivalent circuit across the larger resistance.

For example, if we consider Q=1mW, k_{ox}=4Wm^{-1} K^{-1} [53], k_{Cu}=400 Wm^{-1} K^{-1} and R_1, R_2, R_3 respectively equal to 25 nm, 50 nm and 1µm, the rise in temperature is 404K.

Of course, this is a very rough approximation; if the power dissipated in the sample increases by a factor of 2, 3, 4…ΔT increases by the same factor, letting the sample reach a very high temperature. On the other hand, if the curvature radius of the tip is not small enough, ΔT dramatically drops down and no chemical reactions occur.

Due to the sample composition and because of the thin oxide layer probably formed right under the graphene flake, the same explanation could be extended to the holes formed on graphene. In this case the oxide layer is thinner, but the temperature needed to start chemical reactions should be lower [54].

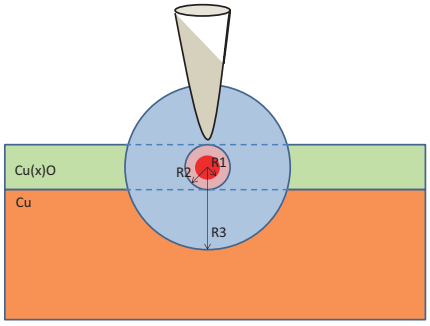

Figure 7. Schematic representation of the heating mechanism due to the microwave near-field. The probe (grey) focuses the power that dissipates into the sample, generating a heat gradient.

Further calculation where performed using electromagnetic calculation (not reported here for space reasons), changing the electrical resistivity of copper oxides. The resistivity at room temperature is in fact 0.5Ωm for CuO and 5Ωm for Cu2O, those values going down to 0.05Ωm for CuO and 0.5Ωm for Cu2O for temperature up to 100°C. Hence, the temperature raise increases the electrical conductivity, and induces a self-focusing effect in the electromagnetic power. Such a focusing effect induces a kind of positive feedback in the reaction, and could help start the patterning effect that we have observed.

For the sake of completeness, we should mention that we have considered and excluded among possible explanations for the patterning effect, a more prosaic possibility, namely a mechanical scratching due to a possible intermittent contact of the tip with the sample. This could be due –for example- to parasitic contribution to the tunneling current by the microwave field at power higher than the commonly used. This explanation was however quickly ruled out, owing to three main indications:

1) the tip is able to perform following STM images keeping the same quality; this is generally not be possible with a tip damaged by occasional contact with the sample;

2) the etching takes a certain minimum time to occur, while modifications of the surface should be immediately visible in case of mechanical scratches;

3) the feedback signal has been accurately monitored, and the current set-point does not show anomalous noise or overshooting during the scan.

VI. Conclusions

In this work, we present high resolutions images of CVD graphene obtained by near-field microwave microscopy and report experimental observation of microwave-induced nanopatterning of graphene flakes. The most likely explanation of the patterning effect is heating-induced oxidation of the exposed graphene flakes. Simple estimates and modeling show that high temperatures under the tip apex are in fact possible, considering self-focusing effects of the electromagnetic field in the copper oxide underneath graphene.

Nonetheless, future work is needed to fully understand the underlying mechanism, and to definitely rule out alternative explanations. Moreover, in order to develop a practically viable microwave-based nanopatterning technique for graphene, different substrates (e.g. silicon oxides) have still to be studied. Finally, microwave power and time of exposure have to be optimized.

Acknowledgment

A portion of this research was conducted at the Center for Nanophase Materials Sciences, which is sponsored at Oak Ridge National Laboratory by the Scientific User Facilities Division, Office of Basic Energy Sciences, and U.S. Department of Energy.

References

[1] Y.-M. Lin, et al., “100-GHz transistor from wafer-scale epitaxial graphene,” Science, vol. 327, is. 5966, pp-662, 2010.

[2] C. Stampfer, et al., “Tunable Coulomb blockade in nanostructured graphene,” Appl. Phys. Lett., vol. 92, is. 012102, pp. 012102-1-3, 2008.

[3] L.A. Ponomarenko, et al., “Chaotic Dirac billiard in graphene quantum dots,” Science, vol. 320, is. 5874, pp. 356-358, 2008.

[4] S. Russo, et al., “Observation of Aharonov-Bohm conductance oscillations in a graphene ring,” Phys. Rev. B, vol. 77, is. 085413, pp. 085413-1-5, 2008.

[5] M. Y. Han, et al., “Energy band-gap engineering of graphene nanoribbons,” Phys. Rev. Lett., vol. 98, is. 206805-1-4, 2007.

[6] C. Berger, et al., “Electronic confinement and coherence in patterned epitaxial graphene,” Science, vol. 312, is. 5777, pp. 1191-1196, 2006.

[7] J. H. Warner, et al., “Structural transformations in graphene studied with high spatial and temporal resolution,” Nat. Nanotech., vol.4, is.8, pp.500-504, 2009.

[8] J. Y. Huang, et al., “In situ observation of graphene sublimation and multi-layer edge reconstructions,” PNAS, vol.106, is.25, pp.10103-10108, 2009.

[9] J. A. Gardener, and J. A. Golovchenko, “Ice-assisted electron beam lithography of graphene,” Nanotech., vol. 23, is. 185302, 6pp, 2012.

[10] I. Childres, et al., “Effect of oxygen plasma etching on graphene studied using Raman spectroscopy and electronic transport measurements,” New J. Phys., vol.13, is. 025008, 12 pp., 2011.

[11] L. Ju, et al., “Graphene plasmonics for tunable terahertz metamaterials,” Nat. Nanotech., vol. 6, is. 10, pp. 630-634, 2011.

[12] M. C. Lemme, et al., “Etching of Graphene Devices with a Helium Ion Beam,” ACS Nano, vol. 3, is. 9, pp. 2674-2676, 2009.

[13] D. Bischoff, et al., “Reactive-ion-etched graphene nanoribbons on a hexagonal boron nitride substrate,” Appl. Phys. Lett., vol.101, is.20, pp.203103-1-4, 2012.

[14] J. G. Son, et al., “Sub-10 nm graphene nanoribbon array field-effect transistors fabricated by block copolymer lithography,” Adv. Mater., to be published, 2013.

[15] S. Kumar, et al., “Reliable processing of graphene using metal etchmasks,” in 11th Trends in Nanotech. Int. Conf. (TNT2010), Nanoscale Res. Lett., 2011.

[16] R. J. Stohr, et al., “All-optical high-resolution nanopatterning and 3D suspending of graphene,” ACS Nano, vol. 5, is. 6, pp. 5141-5150, 2011.

[17] Y.-L. Zhang, et al., “Designable 3D nanofabrication by femtosecond laser direct writing,” Nano Today, vol. 5, pp. 435-448, 2010.

[18] J.A. Leon, et al., “Rapid fabrication of bilayer graphene devices using direct laser writing photolithography,” J. Vac. Sci. Technol. B, vol. 29, is.2, pp. 021204-021204-7, 2011.

[19] W. S. Lim, et al., “Atomic layer etching of graphene for full graphene device fabrication,” Carbon, vol. 50, is. 2, pp. 429-435, 2012.

[20] T. Tsukamoto, and T. Ogino, “Control of graphene etching by atomic structures of the supporting substrate surfaces,” The Journ. of Phys. Chem. C, vol. 115, is. 17, pp. 8580-8585, 2011.

[21] L. C. Campos, et al., “Anisotropic etching and nanoribbon formation in single-layer graphene,” Nano Letters, vol. 9, is. 7, pp. 2600-2604, 2009.

[22] J. Cai, et al., “Atomically precise bottom-up fabrication of graphene nanoribbons,” Nature, vol 466, is. 7305, pp. 470-473, 2010.

[23] Y. Xueqiu, and J. J. Pak, “Lithography-free fabrication of bistability graphene FET biosensor,” Nanotechnology (IEEE-NANO), 2011 11th IEEE Conference on, pp.617-620, 15-18 Aug. 2011.

[24] C. X. Cong, et al., “Fabrication of graphene nanodisk arrays using nanosphere lithography,” The Journ. Of Phys. Chem. C, vol. 113, is. 16, pp. 6529-6532, 2009.

[25] M. Wang, et al., “CVD growth of large area smooth-edged graphene nanomesh by nanosphere lithography,” Sci. Rep., vol. 3, 2013.

[26] A. Fasoli, et al., “Fabrication of graphene nanoribbons via nanowire lithography,” phys. stat. sol. (b), vol. 246, is. 11-12, pp. 2514-2517, 2009.

[27] X. Liang, et al., “Formation of bandgap and subbands in graphene nanomeshes with sub-10 nm ribbon width fabricated via nanoimprint lithography,” Nano Letters, vol. 10, is. 7, pp. 2454-2460, 2010.

[28] X. Wang, and H. Dai, “Etching and narrowing of graphene from the edges,” Nat. Chem., vol. 2, is. 8, pp. 661-665, 2010.

[29] M. Haydell, et al., “Direction writing of graphene-based nanoribbons via thermochemical nanolithography,” Microsystems for Measurement and Instrumentation (MAMNA), 2012 , pp.1-3, 27 March 2012.

[30] S. Zhao, et al., “Photochemical oxidation of CVD-grown single layer graphene,” Nanotech., vol. 23, is. 35, pp. 355703-355703-6, 2012.

[31] S. Prezioso, et al., “Large area extreme-UV lithography of graphene oxide via spatially resolved photoreduction,” Langmuir, vol. 28, is. 12, pp. 5489-5495, 2012.

[32] S. Neubeck, et al., “Scanning probe lithography on graphene,” phys. stat. sol. (b), vol. 247, is. 11-12, pp. 2904-2908, 2010.

[33] W. Zhang, et al., “Direct writing on graphene 'paper' by manipulating electrons as 'invisible ink',” Nanotech., vol. 24, is. 27, pp. 275301-275301-6, 2013.

[34] L. Tapaszto, et al., “Tailoring the atomic structure of graphene nanoribbons by scanning tunnelling microscope lithography,” Nat. Nanotech., vol. 3, is. 7, pp. 397-401, 2008.

[35] I.-S. Byun, et al., “Nanoscale lithography on monolayer graphene using hydrogenation and oxidation,” ACS Nano, vol. 5, is. 8, pp. 6417-6424, 2011.

[36] L. Weng, et al., “Atomic force microscope local oxidation nanolithography of graphene,” Appl. Phys. Lett., vol. 93, is. 9, pp.093107-093107-3, 2008.

[37] A.J.M. Giesbers, et al., “Nanolithography and manipulation of graphene using an atomic force microscope,” Sol. State Comm., vol. 147, is. 9–10, pp. 366-369, 2008.

[38] Y.-S. Shin, et al., “High-mobility graphene nanoribbons prepared using polystyrene dip-pen nanolithography,” J. of the Am. Chem. Soc., vol. 133, is. 15, pp. 5623-5625, 2011.

[39] P. Pingue. “Scanning probe based nanolithography and nanomanipulation on graphene,” in Tip-Based Nanofabrication, Springer, New York, ch. 10, pp. 357-386, 2011.

[40] Nanofabrication device and method for manufacture of a nanofabrication device, by M. Tabib-Azar. (2012, Oct 11). Patent US 2012/0255932, [Online], Available: http://www.freepatentsonline.com/y2012/0255932.html.

[41] M. Farina, et al., “Fast ultrahigh-density writing of low-conductivity patterns on semiconducting polymers”, Nature Commun.., 4:2668, doi: 10.1038/ncomms3668 (2013)

[42] T. Monti, et al., “Graphene etching by a near-field scanning microwave microscope,” in Int. Microw. Symp. 2013 (IMS2013), June , 2013.

[43] M. Farina, et al., “Disentangling time in a near-field approach to scanning probe microscopy,” Nanoscale, vol. 3, is. 9, pp.3589-3593, 2011.

[44] T. Monti, et al., “Near-field microwave investigation of electrical properties of graphene-ITO electrodes for LED applications,” J. Display Technol., vol. 9, is. 6, pp. 504-510, 2013.

[45] A. Tselev, et al., “Near-field microwave microscope with improved sensitivity and spatial resolution,” Rev. Sci. Instrum., vol. 74, is.6, pp. 3167-3170, 2003.

[46] M. Farina, et al., “Tomographic effects of near-field microwave microscopy in the investigation of muscle cells interacting with multi-walled carbon nanotubes,” Appl. Phys. Lett., vol. 101, is. 20, pp. 203101-203101-4, 2012.

[47] V. V. Talanov, et al., “A near-field scanned microwave probe for spatially localized electrical metrology,” Appl. Phys. Lett., vol. 88, is. 13, pp. 134106-134106-3, 2006.

[48] J. Lee, et al., “Atomic resolution imaging at 2.5 GHz using near-field microwave microscopy,” Appl. Phys. Lett., vol. 97, is. 18, pp. 183111-183111-3, 2010.

[49] I. Vlassiouk, et al., “Role of hydrogen in chemical vapor deposition growth of large single-crystal graphene.” ACS Nano, vol. 5, is. 7, pp. 6069-6076, 2011.

[50] M. Schriver, et al., “Graphene as a long-term metal oxidation barrier: worse than nothing,” ACS Nano, to be published (available online 7 June 2013).

[51] Y. Zhang, et al., “Defect-like structures of graphene on copper foils for strain relief investigated by high-resolution scanning tunneling microscopy,” ACS Nano, vol. 5, is. 5, pp. 4014-4022, 2011.

[52] T. L. Bergman, et al., Fundamentals of heat and mass transfert, John Wiley & Sons. Inc., pp. 141-142, 7th Ed., 2011.

[53] A. Kusiak, et al., “CuO thin films thermal conductivity and interfacial thermal resistance estimation,” The Europ. Phys. J. Appl. Phys., vol. 35, is. 1, pp 17-27, 2006.

[54] L. Liu, et al., “Graphene oxidation: thickness-dependent etching and strong chemical doping,” Nano Letters, vol. 8, is. 7, pp. 1965-1970, 2008.

View publication stats